





Article

Cell Response on Laser-Patterned Ti/Zr/Ti and Ti/Cu/Ti Multilayer Systems

Suzana Petrović ^{1,*}, Nevena Božinović ¹, Vladimir Rajić ¹ , Danijela Stanisavljević Ninković ² , Danilo Kisić ¹, Milena J. Stevanović ^{2,3,4}  and Emmanuel Stratakis ⁵ 

- ¹ Vinča Institute of Nuclear Sciences, University of Belgrade, P.O. Box 522, 11001 Belgrade, Serbia; nevena.bozinovic@vin.bg.ac.rs (N.B.); vladimir.rajic@vin.bg.ac.rs (V.R.); dankisic@vin.bg.ac.rs (D.K.)
- ² Institute of Molecular Genetics and Genetic Engineering, University of Belgrade, Vojvode Stepe 444a, P.O. Box 152, 11042 Belgrade, Serbia; danijelastanisavljevic@imgge.bg.ac.rs (D.S.N.); milenastevanovic@imgge.bg.ac.rs (M.J.S.)
- ³ Faculty of Biology, University of Belgrade, Studentski trg 16, P.O. Box 43, 11000 Belgrade, Serbia
- ⁴ Serbian Academy of Sciences and Arts, Knez Mihailova 35, 11001 Belgrade, Serbia
- ⁵ Institute of Electronic Structure and Laser (IESL), Foundation for Research and Technology (FORTH), N. Plastira 100, Vassilika Vouton, 70013 Heraklion, Crete, Greece; stratak@iesl.forth.gr
- * Correspondence: spetro@vin.bg.ac.rs; Tel.: +381-11-3408560

Abstract: Arranged patterns obtained via ultrafast laser processing on the surface of Ti/Cu/Ti/Si and Ti/Zr/Ti/Si thin-film systems are reported. Two differently designed multilayer thin films Ti/Cu/Ti/Si and Ti/Zr/Ti/Si were deposited on silicon using the ion sputtering method. The bioactive surfaces of these systems involve the formation of laser-induced periodic surface structures (LIPSS) in each of the laser-written lines of mesh patterns on 5 × 5 mm areas. The formation of nano- and micro-patterns with an ultra-thin oxide film on the surfaces was used to observe the effects of morphology and proliferation of the MRC-5 cell culture line. To determine whether Ti-based thin films have a toxic effect on living cells, an MTT assay was performed. The relative cytotoxic effect, as a percentage of surviving cells, showed that there was no difference in cell number between the Ti-based thin films and the control cells. There was also no difference in the viability of the MRC-5 cells, except for the Ti/Cu/Ti/Si system, where there was a slight 10% decrease in cell viability.

Keywords: multilayer thin films; laser modification; laser-induced periodical surface structure LIPSS; cell response



Citation: Petrović, S.; Božinović, N.; Rajić, V.; Stanisavljević Ninković, D.; Kisić, D.; Stevanović, M.J.; Stratakis, E. Cell Response on Laser-Patterned Ti/Zr/Ti and Ti/Cu/Ti Multilayer Systems. *Coatings* **2023**, *13*, 1107. <https://doi.org/10.3390/coatings13061107>

Academic Editors: Ajay Vikram Singh and Rafael Comesaña

Received: 28 April 2023

Revised: 3 June 2023

Accepted: 14 June 2023

Published: 16 June 2023



Copyright: © 2023 by the authors. Licensee MDPI, Basel, Switzerland. This article is an open access article distributed under the terms and conditions of the Creative Commons Attribution (CC BY) license (<https://creativecommons.org/licenses/by/4.0/>).

1. Introduction

Implants are now becoming a standard therapy for repairing and replacing bone tissue, making daily activities much easier for patients. The implanted biomaterial should replace the missing bone while stimulating osteoconduction for bone re-growth. On the one hand, extensive research has been directed at improving the performance of implants in terms of biocompatibility and satisfactory mechanical properties [1,2]. New alloys have been developed, mainly based on titanium. On the other hand, surface modifications, such as the adaptation of the chemical composition of the contact surface and the formation of specific morphological features at the micro- and nanometer levels, further improve the performance of the implant. It has been shown that micro- and nanostructured surfaces are a good way to improve the bioactivity of biomaterials and the osteogenic differentiation of cells [3].

Metal orthopedic implants were considered more promising due to their greater toughness and durability, but a large number of metals and their alloys, although possessing desirable bactericidal properties, can be very irritating and toxic in contact with the biological environment [4]. Orthopedic materials such as steel, titanium alloys (Ti-6Al-4V one of the most commonly used), and chromium alloys are widely used as orthopedic

implants and devices, which have been adopted for dentistry and hard tissue reconstructive surgery. However, there are some unwanted side effects that occur, such as a tendency to corrosion, insufficient biocompatibility, and subsequent tissue irritation, which limit their application [5,6]. The continuous development of materials for orthopedic implants requires knowledge of their mechanical and microstructural properties, as well as the development of new methods of surface modification in order to adapt the morphology to the best possible cellular response. To obtain the large-scale incorporated layer (antibacterial or more biocompatible) in order to avoid the exfoliation from the substrate, a relatively new surface modification technology called friction stir processing (FSP) was developed to produce a surface nanocomposite with enhanced mechanical properties in many alloy systems [7]. In addition, one promising technique is selective laser melting (SLM) for manufacturing Ti-based alloys composed of dense blocks that have advantages such as low porosity and high yield strength, and in which the element segregation is suppressed significantly. This method has allowed for the formation of strut-based latticed-beams structures with a tunable Young's modulus, which is applicable to the complex bone structure [8].

Titanium (Ti)-based materials are good biomaterials due to their properties, such as biocompatibility, light weight, high strength, and superior corrosion resistance [9,10]. For long-term bone replacements, titanium alloys should possess bone-mimicking mechanical properties, which can be obtained by the optimization of the geometry of the porous structure. Topologically porous Ti-based implants also improve osseointegration and can be made patient-specific, which is essential for preventing their failure due to the inadequate integration of the implant into the bone tissue [11]. Titanium alloys are suitable as biomaterials due to their superior biocompatibility, as the outer oxide layer is negatively charged at physiological pH and the soluble metal components cannot be released into the biological fluids [12,13]. A high concentration of β -stabilizing elements in Ti-based alloys has been developed as a potential solution to the mismatch between the elastic modulus of the implant and the surrounding bone tissue. Zirconium (Zr) is the most common element added to Ti alloys, as it does not show any cytotoxic reaction when in contact with cells [14–16]. The crucial part of the biomaterial's application is the formation of the implant–tissue interface during the interaction between the Ti alloy and the biological environment, which is largely defined by the surface characteristics of the alloy. Surface topography, composed of micro- and nanometer features, determines cell adhesion, morphology, proliferation, and differentiation, and therefore has a major impact on cell survival and implant–tissue interface properties [17]. Recently, the Ti–Nb–Zr–Ta alloy has attracted more and more attention due to the shape memory effect and superelastic behavior is associated with a reversible, thermoelastic transformation between the β phase and the α' martensite phase of the alloy [18]. Ikarashi et al. implanted Ti, Zr, and Ti–Zr alloy into rats for 8 months, and no toxicological or weight changes in the body or organ, as well as in hematological parameters, were observed. However, the tissue inflammatory responses to the Ti–Zr alloy were lower and the Ti–Zr alloy had better biocompatibility than other artificial surgical implants [19]. In preclinical studies, the Ti–Zr alloy, in combination with a SLActive® surface (Straumann's high-performance surface with extensive healing potential), is a suitable material for small-diameter implants. The results demonstrated good performance and tolerability with high implant stability and fast osseointegration [20,21].

Metallic orthopedic materials, as a substitute for hard tissue in clinical use, can release metallic ions and wear debris in artificial joints, and these are serious problems that need to be solved for safe application. Essentially, metals are non-biofunctional; their surfaces should be modified to improve corrosion resistance, wear resistance, and bone conductivity [1]. The surface modification of orthopedic material aims to enhance its performance in contact with the biological environment by forming a biointerface. Frequently used surface techniques are physicochemical methods that alter surface characteristics by physical texturing and/or chemical reactions including etching/oxidation, the addition of functional groups, deposition of functional thin films, ion or laser irradiation treatments, and surface patterning by lithography [22]. Among a variety of surface modification techniques, the

ultrafast laser modification technique has emerged as one of the best for forming ordered surface patterns, increasing surface roughness, changing composition, and functionalizing and forming a thin film [23]. This technique is suitable for the fabrication of bioactive surfaces on stents, bone implants, and biofilms [24–26]. The energy of laser radiation can be focused on the surface and can modify only selected areas, triggering the transformation of hardening, surface melting, surface oxidation, and/or surface alloying [27].

The laser processing of biomaterials is a particularly important opportunity for the application of multiple pulsed laser effects that produce laser-induced periodic surface structures (LIPSS). When the periodicities of LIPSS are nearly equal to the laser wavelength and are oriented normal to the polarization vector of the laser radiation, they are referred to as low spatial frequency LIPSS (LSFL) [28,29]. Another type of periodic structure, called high-spatial-frequency LIPSS (HSFL), has a much lower spatial periodicity but is aligned parallel to the polarization vector [30]. Advances in the field of ultrafast laser processing, based on the ablation of materials, are very important due to the generation of 2D-surface and 3D-volume micro- and nanopatterns. One of the main advantages of ultrafast laser pulses for ablating materials is that they are capable of producing extremely high peak radiation intensities ($>10^{11}$ W/cm²), generating free electrons through a multiphoton absorption mechanism and band-gap tunnelling. A high density of excited electrons can be created locally in a small focal volume due to nonlinear absorption, triggering avalanche ionization that supports plasma formation. Consequent to that is the fabrication of a smoother cavity wall with negligible thermal damage [31,32]. Recently, ultrafast laser surface modification has evolved into a unique method that enables the fabrication of a bioactive surface with the formation of the desired oxide and alloy, the generation of nano/microtextures, and the modification of the wettability of the surface [33–36]. The optimal surface structure can be achieved through different surface patterns (physical shape and size, roughness, regular or irregular series of patterns, wettability, surface energy, etc.), with appropriate surface composition (oxides that prevent the release of toxic metal ions), in order to stimulate cell growth.

The main aim of this work is to investigate the possibility of obtaining bioactive surfaces on Ti/Zr/Ti/Si and Ti/Cu/Ti/Si systems, with adapted morphology and wettability for cell integration. The reason for choosing the Ti/Zr/Ti/Si and Ti/Cu/Ti/Si systems is reflected in the fact that titanium alloys with Zr have a satisfactory mechanical strength and good corrosion resistance in biological fluids, and their biocompatibility is better than commercially pure Ti for implants [37]. On the other hand, copper, as an essential trace element required for human health, is one of the most promising alloying elements for clinical applications due to its low toxicity and high cytocompatibility. Recently, several studies have reported that titanium alloys with Cu have excellent antibacterial function [38]. It was reported that Ti-(1 wt.% and 5 wt.%) Cu alloys showed antibacterial properties with an antibacterial rate of about 30% in comparison with pure titanium [39]. Precisely, Zr and Cu are present in small amounts just below the surface, so that after laser modification they are in contact with the biological environment. The research focused on the formation of laser-printed templates with micro- and nanometer dimensions and inherent wettability suitable for the positioning of cells to enable their proliferation and growth. The systematization of the obtained results included a comparison of the changes in the Ti/Zr/Ti/Si and Ti/Cu/Ti/Si systems deposited and modified under the same experimental conditions. Specifically, the results were intended to show the influence of the type of alloy component added to the Ti matrix on the properties of the bioactive surface. The MTT test will show the degree of cell survival on different Ti/Zr/Ti/Si and Ti/Cu/Ti/Si systems with almost the same surface topography.

2. Materials and Methods

Thin-film deposition. The thin multilayer films of Ti/Cu/Ti/ and Ti/Zr//Ti were deposited on the single crystal (100) of n-type silicon in a Balzers Sputtron II system via ion sputtering of pure Ti, Cu, and Zr with 1.3 keV argon ions. Before chamber assembly,

the surfaces of the Si substrates were cleaned with ethanol and dilute hydrofluoric acid (HF) to remove impurities and native Si oxides. The base pressure in the chamber was 5.5×10^{-4} Pa. Targets were sputtered with a constant current of 0.7 A and a voltage of 0.5 kV for Ti, and corresponding current and voltage values of 0.5 A and 1.2 kV for the deposition of Cu and Zr, respectively. The deposition rates were constant at about 0.13 nm s^{-1} for Ti and 0.25 nm s^{-1} for Cu and Zr. The total thickness of the deposited Ti/Cu/Ti and Ti/Zr//Ti thin films was 300 nm, with the subsurface Cu and Zr layers having a thickness of 10 nm and the top Ti layer also having a thickness of 10 nm.

Ultra-fast laser modification. The laser processing of these specific Ti/Zr/Ti/Si and Ti/Cu//Ti/Si systems was performed using the Yb: KGW laser source Pharos SP from Light Conversion. The surfaces of the thin films were irradiated with focused, linear p-polarized pulses with the following characteristics: repetition rate of 5 kHz, pulse duration equal to 160 fs, and central wavelength of 1026 nm. The joulemeter is used to measure the energy deposited on the surface of the sample before real irradiation. In each irradiation, the pulse energy was assumed to be constant (with value of 1.5 μJ), as the deviation of the pulse energy was less than 1%. The laser beam pulses were guided through proper optical mirrors and an optical lens and focused on the sample surface with an $f = 200$ mm plano-convex lens. The beam diameter was characterized using a CCD camera close to the focal plane and was estimated at around $\sim 60 \mu\text{m}$ for the Gaussian beam, with a corresponding spot size at a focus of $2.8 \times 10^{-5} \text{ cm}^2$ (spot diameter 30 μm). Irradiations were performed with a fluence of $0.110 \pm 0.005 \text{ J cm}^{-2}$ (calculated as $\Phi_0 = 2E_p/\pi\omega_0^2$ with E_p the pulse energy and ω_0 the beam radius at $1/e^2$). The samples were laser processed in the open air and mounted on a motorized computer-controlled X-Y-Z translation perpendicular to the laser beam. The irradiation strategy included the formation of mesh at the surface of sample $5 \times 5 \text{ mm}$ composed of laser-printed lines at a scanning speed of 15 mm s^{-1} (20 pulses per spot). Firstly, the lines of 5 mm length are drawn at a distance of 75 μm ; then, the sample is turned 90° and the procedure is repeated so that finally a mesh of laser-printed lines is obtained.

Morphological characterization. The surface morphology and microstructure of the Ti/Zr/Ti/Si and Ti/Cu/Ti/Si thin films before and after laser processing were analyzed by a FESEM, FEI SCIOS 2 Dual Beam scanning electron microscope (SEM, Thermo Fisher Scientific, Waltham, MA, USA) equipped with an energy-dispersive X-ray spectroscope (EDS) at 10 kV of acceleration voltage.

Surface free energy (SFE) determination using the sessile drop method. The wettability measurements were performed using a home-made device equipped with a polychromatic LED lamp as a counter light source (YINYAN MODEL TECH. LTD, Shenzhen, China), and a USB digital CCD camera (König Electronic USB microscope, model CMP-usbmicro10, König Electronic, Jiangsu, China). The working distance between the lens and the sample holder was 15 mm, with a magnification of $36\times$ for the diagonal field of view of 8 mm, while the scale bar length is 100 ± 1 pixels per millimeter. The basic data in this study were the contact angle (CA— θ), which indicates the degree of wetting as the contact between the surface and the liquid. The CA with the surface of the samples on untreated and laser-treated thin films was measured at a room temperature of 23°C and a relative humidity of 53%–56% with three different liquid drops (water, ethylene glycol, diiodomethane). Droplets were laid on the surfaces of samples using a micropipette, and the droplet volume was set to 3 μL . To obtain the average value, contact angle measurements were taken from at least six separate regions of the same sample. Image analysis was performed with public ImageJ software [40]. The SFE and its polar (γ_p) and dispersive components (γ_d) of the metallic surfaces were calculated using the Good–van Oss model based on the contact angle data [41].

Study of cellular response. MRC-5 cells (ATCC[®], CCL-171TM, Manassas, VA, USA) were maintained in Dulbecco's Modified Eagle's Medium (DMEM) supplemented with 10% fetal bovine serum (FBS), 4500 mg/L glucose, 2 mmol/L L-glutamine, and antibiotic/antimycotic (all from Invitrogen[™], Grand Island, NY, USA) at 37°C and 10% CO_2 .

Cells were observed and images were acquired using a DM IL LED inverted microscope (Leica Microsystems, Wetzlar, Germany). Two pieces of each thin film (Ti, Ti/Cu/Ti, and Ti/Zr/Ti) with a size of 10 mm × 10 mm were incubated with DMEM culture medium under sterile conditions at 37 °C and 10% CO₂ for 10 days. After incubation, the thin film was removed, and the remaining medium was considered to be 100% extract. A diluted extract (50% and 15%) was used for experiments.

The indirect method was used to measure the cytotoxicity of the film. MRC-5 cells were grown at a density of 10,000 cells on a 96-well plate and cultured the next day with 100%, 50%, and 15% of the extraction medium obtained from the incubated films with DMEM for 10 days at 37 °C. After 24 h of incubation, cell viability was determined using the MTT (3-(4,5-dimethylthiazol-2-yl)-2,5-diphenyltetrazolium bromide) assay according to the manufacturer's protocol. Absorbance was measured at 540 nm using an Infinite 200 pro plate reader (Tecan, Austria). Two controls were used: MRC-5 cells treated with DMEM and incubated at 37 °C for 10 days without films (referred to as Blank), and MRC-5 cells treated with fresh DMEM (referred to as C). As a positive control for cytotoxicity, we used MRC-5 cells treated with pyrimethanil (denoted as P), for which the cytotoxic effect on MRC-5 cells has been previously demonstrated [42]. Statistical analyses were performed using SPSS statistical software (version 20). The results obtained are means ± SEM from four independent experiments. Statistical analyses were performed using Student's *t*-test, and a *p*-value ≤ 0.05 was considered significant, with *p* ≤ 0.05 denoted as *.

3. Results and Discussion

Morphological Characterization of Ti/Zr/Ti/Si and Ti/Cu/Ti/Si Thin-Film Systems

Femtosecond multipulse laser exposure to Ti/Zr/Ti/Si and Ti/Cu/Ti/Si thin-film systems was used to create a regular mesh of laser-printed lines forming micrometer-sized morphological features. To achieve a suitable position of the cells on the surface, the diameter of the laser beam was set to about 30 μm, while the distance between the lines was about 75 μm [43]. The morphological characteristics of the Ti/Zr/Ti/Si thin-film system after laser processing were analyzed using the SEM method (Figure 1). Laser-induced periodic surface structures (LIPSS) aligned normally to the polarization vector of the applied laser beam are formed in each laser-printed line, which classifies them as low spatial frequency LIPSS (LSFL) [28,29]. The formation of LSFL was accompanied by some degree of material removal, which contributed to their well-defined shape, especially at the intersections (Figure 1). Nanoparticles of size 70–150 nm accumulated at the edges of the lines, which is due to the pronounced ablation during the formation of the periodic structure in the central part. In the crossing region, the LSFLs are narrow and densely distributed with a spatial periodicity of about 700 nm. On the other hand, the spatial periodicity of the ripple structure in the lines was about 1 μm (very close to the laser wavelength), meaning the LSFLs are more widely and less frequently distributed (Figure 1). The square inner regions between the lines, which are not processed by the laser, are partially covered with nanoparticles.

The Ti/Cu/Ti/Si system was modified under the same experimental laser processing conditions as the Ti/Zr/Ti/Si system. In general, the observed morphological features are similar to the previous case (Figures 1 and 2), except for some details: (i) the width of the laser-printed line is narrower, which is a consequence of the less pronounced ablation of the material; (ii) the periodic structure (LSFL) in the line is not well defined due to the occurrence of hydrodynamic effects in the form of partial surface melting; (iii) among the unclear LSFL ripples, the additional appearance of high-spatial-frequency LIPSS (HSFL) with a periodicity below 200 nm and an orientation parallel to the polarization is observed; and (iv) at the edges of the lines, there is no large number of nanoparticles, which is probably due to the effect of surface melting (Figure 2). It is interesting to note that the Cu sublayer with a thickness of 10 nm significantly reduces the ablation effect, which is due to the thermophysical properties of Cu and Zr [44,45]. The higher mobility of Cu atoms, as

well as the higher thermal conductivity of copper, may contribute to an easier redistribution of the absorbed laser radiation energy in the Ti/Cu/Ti/Si system.

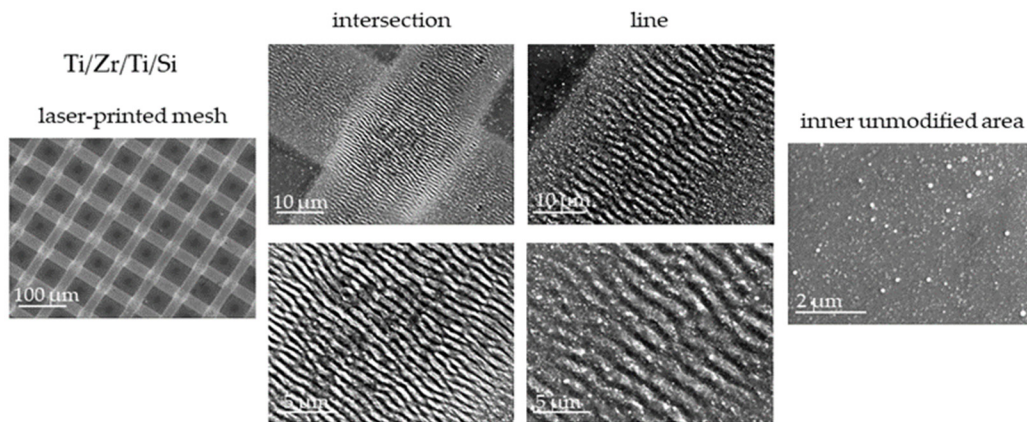


Figure 1. SEM micrographs after laser-printed line mesh on the surface of Ti/Zr/Ti/Si thin-film system with morphological details at an intersection, line, and inner unmodified areas.

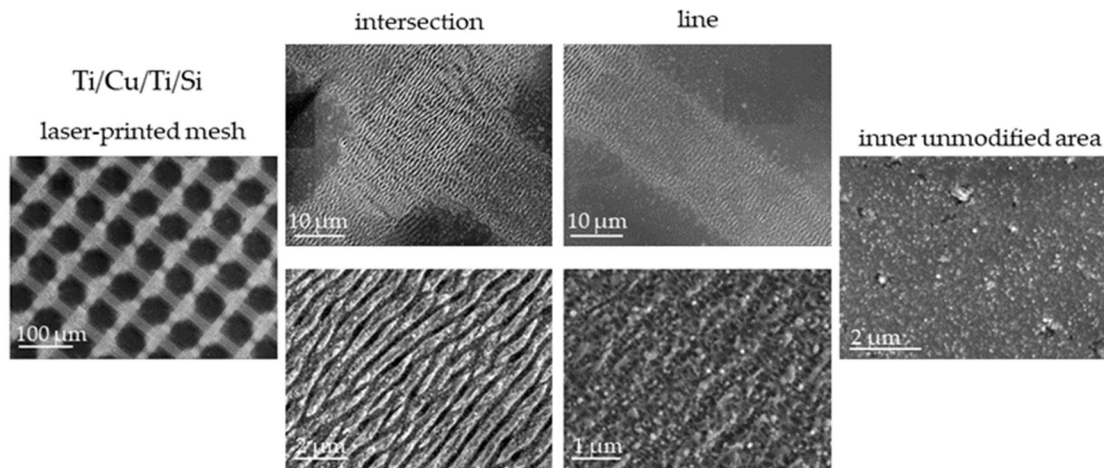


Figure 2. SEM micrographs after laser-printed line mesh on the surface of Ti/Cu/Ti/Si thin-film system with morphological details at an intersection, line, and inner unmodified areas.

The mapping of the laser-modified surface for both systems studied was performed using EDS and is shown in Figure 3. The distribution of the thin-film components (Ti, Zr or Cu, Si, and O) follows the pattern of a laser-printed mesh, which superficially appears very similar for both systems.

In the individual elemental maps for Ti and Si in both systems, it can be seen that the ablation is more intense in the Ti/Zr/Ti/Si system, which is due to the presence of a larger number of Si atoms at the positions of the laser-printed lines, and, in particular, at the intersection positions (Figure 3a,b). In the Ti/Cu/Ti/Si system on the elemental map for Ti, deviations from the uniform distribution of Ti were observed only at the intersection points (Figure 3b). Comparing the distribution of Zr and Cu on the corresponding elemental maps (Figure 3a,b), it was found that the ablation of Zr is much more pronounced in the laser-printed lines, which is evident in a larger area where the concentration of the Zr component is reduced. However, the ablation is not complete at the locations of the laser-printed lines because the ablated material is redeposited in the form of nanoparticles. There was additional ablation in the intersections, so the presence of Zr or Cu components is not expected. The oxygen is mostly uniformly distributed over the surface in both sample types, and originates from laser-induced surface oxidation or atmospheric contamination. In the Ti/Cu/Ti/Si samples, a slightly higher oxygen concentration is observed at the positions

of the laser-printed lines, suggesting that a lower ablation of the material is associated with a more intense surface oxidation of the Ti and Cu species.

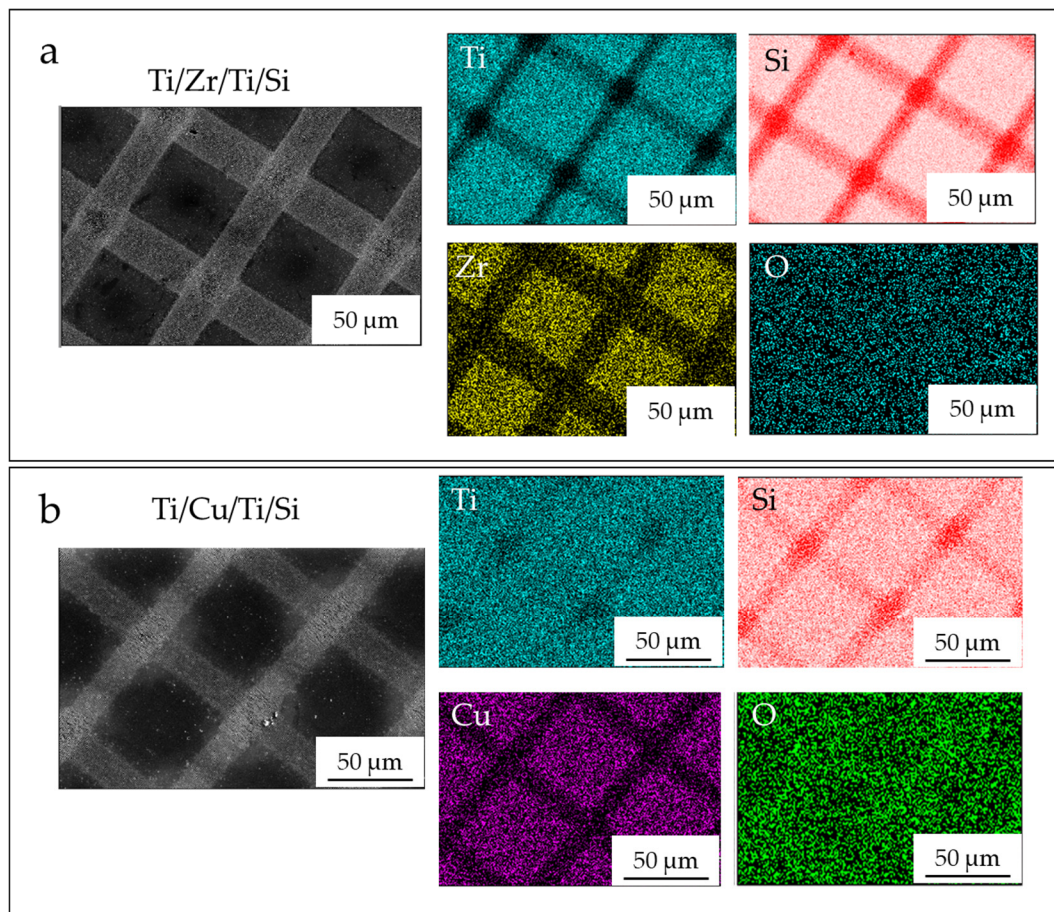


Figure 3. EDS mapping of the laser-modified surface for (a) Ti/Zr/Ti/Si and (b) Ti/Cu/Ti/Si thin-film systems, with corresponding elemental maps.

A comparison was also made of the concentrations at specific points corresponding to the unmodified area (as deposited), the inner unmodified area (center), the laser-printed lines, and the intersection areas, as shown in Tables 1 and 2. In the Ti/Zr/Ti/Si system, significantly higher material removal (more than 30%) was obtained, and no Cu or Zr sublayer components were present at the intersections. The higher concentration of Ti after modification was achieved by normalizing the concentration of the components in the analyzed information volume of the sample. During laser irradiation, slightly more Cu remained in the lines than Zr. The results indicate that oxygen from the atmosphere more readily oxidized the surface where copper was present. Taking into account the current and previous studies of a similar Ti/Zr multilayer system, it can be concluded that a larger fraction of the laser pulse energy delivered to the system induces intense ablation (removal of between 100 and 200 nm thin film), while a smaller fraction of the absorbed energy induces changes in the composition, coinciding with a change in the lattice temperature (in-depth about 50 nm) based on the numerical simulation of the temperature profile [36,46,47].

Table 1. Concentrations (weight %) of Ti, Si, Zr, and O species in the Ti/Zr/Ti/Si sample at the positions of the unmodified part (as-deposited), the inner unmodified part (center), laser-printed lines, and intersection regions.

Ti/Zr/Ti/Si	Ti	Si	Zr	O
As-deposited	77.03	16.21	5.81	0.95
Center	76.60	16.75	5.67	0.98
Line	49.37	47.88	0.74	2.01
Intersection	43.91	53.63	/	2.46

Table 2. Concentrations (at %) of Ti, Si, Cu, and O species in the Ti/Cu/Ti/Si sample at the positions of the unmodified part (as-deposited), the inner unmodified part (center), laser-printed lines, and intersection regions.

Ti/Cu/Ti/Si	Ti	Si	Cu	O
As-deposited	72.92	14.85	10.91	1.32
Center	73.09	15.04	10.51	1.36
Line	74.37	17.92	5.08	2.63
Intersection	74.62	22.35	/	3.03

Surface free energy (SFE) can be considered a quantity that characterizes the affinity of a surface for other materials (e.g., liquids). Contact angle measurements were used to study the Ti-based thin films, as-deposited and after laser treatment using deionized water, ethylene glycol, and diiodomethane as reference fluids. The SFE (γ_s) contains dispersive γ_s^d (Lifshitz–Van der Waals) and polar γ_s^p (Lewis acid γ_s^+ and base γ_s^-) components related by the equation [48]. Based on the results in Table 3, where the average contact angle values are given, it can be observed that all samples had higher contact angles after laser irradiation and the best possible wettability for diiodomethane was achieved.

Table 3. Surface free energy (SFE) (γ_s) and its components, and dispersive contact angles of the films wetted with deionized water and diiodomethane.

Specimen	Contact Angle [°]			Surface Free Energy [mJ/m ²]		
	Deionized Water	Diiodomethane	Ethylene Glycol	Polar Part (γ_s^p)	Nonpolar Part (γ_s^d)	Total (γ_s)
Ti/Cu/Ti as-prepared	84 ± 3	50 ± 3	54 ± 2	1.7	33.7	35.4
Ti/Cu/Ti laser modified	86 ± 4	51 ± 3	63 ± 3	0.6	34.3	34.9
Ti/Zr/Ti as-prepared	82 ± 2	37 ± 2	58 ± 3	3.3	40.1	43.4
Ti/Zr/Tu laser modified	86 ± 3	40 ± 2	70 ± 3	6.3	40.1	46.4

The dispersive component was much more pronounced in all samples than the polar component, which did not change after irradiation. This proportion of surface energy components indicates that the sample surfaces have a stronger preference for nonpolar organic liquids than for water. Surface hydrophobicity is primarily due to the self-association of water molecules upon contact with a nonpolar surface. Accordingly, surface hydrophobicity (water un-wettability) refers to the poor solubility of nonpolar solutes, such as hydrocarbons, in water according to the rule of equality [49]. From Table 3, it can be seen that the value of total SFE slightly increases for the Ti/Zr/Ti/Si layer, which means that the laser irradiation did not significantly change the dispersive character of the surfaces, even though the removal was more severe compared to the Ti/Cu/Ti/Si layer.

Therefore, Table 4 explains in more detail how the surface changes after laser processing. While the Lewis acid component dominates in the laser-modified Ti/Zr/Ti/Si, the Lewis base component predominates in both irradiated samples, indicating that chemical species containing only one electron pair became dominant after laser treatment. This

could be the result of the increase in surface oxygen concentration and the formation of oxygen-containing species, which was confirmed by the SEM (EDS) method.

Table 4. Calculated values of the Lewis acid γ_s^+ and Lewis base γ_s^- components.

Sample	γ_s^+ [mJ/m ²]	γ_s^- [mJ/m ²]
Ti/Cu/Ti as-Prepared	0.77 ± 0.03	0.92 ± 0.03
Ti/Cu/Ti laser modified	0.02 ± 0.04	4.82 ± 0.03
Ti/Zr/Ti as-prepared	0.29 ± 0.02	9.14 ± 0.02
Ti/Zr/Tu laser modified	1.30 ± 0.03	7.53 ± 0.02

The wettability of Ti/Zr/Ti/Si and Ti/Cu/Ti/Si surfaces was investigated using CA measurements before and after laser treatment. Using Image J Drop Analysis software, the wetting angles were calculated with deionized water, diiodomethane, and ethylene glycol, and shown in the images in Figures 4 and 5. It can be seen that the surfaces of both samples are hydrophobic after laser irradiation, taking into account that the contact angles with water are slightly larger than before. Following Berg's limits based on the measurements of hydrophobic forces [50,51], it can be concluded that the Ti/Zr/Ti/Si and Ti/Cu/Ti/Si thin films are supported by hydrophobic forces and are less water wettable. Due to the energetically beneficial displacement of solutes from the solution into the interphase between solid and solute phases, hydrophobic surfaces facilitate the adsorption of various surfactants and proteins from water [52]. When important measures of biological activity responsive to interfacial phenomena are related to the water adhesion tension of the contacting surfaces, it becomes clear that the physicochemical properties of the interfacial water have a strong influence on the biological response to materials.

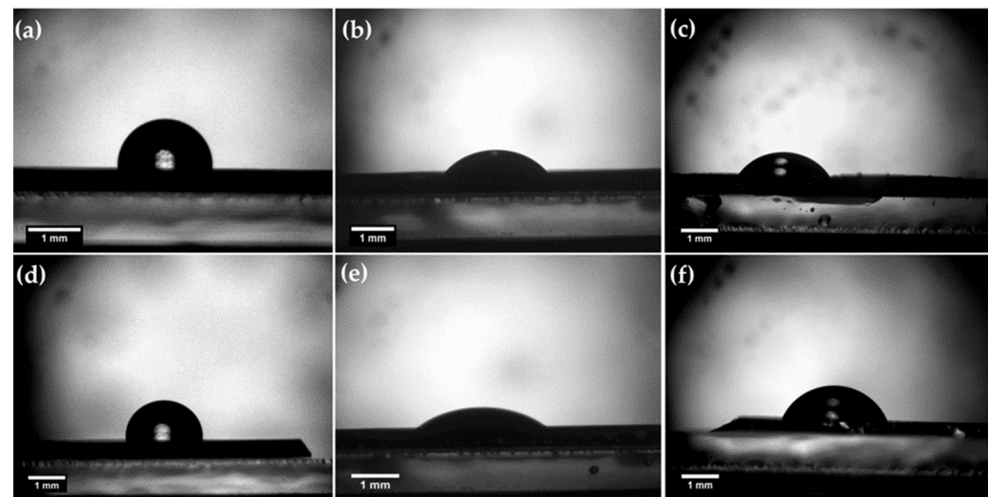


Figure 4. Static behavior of 3 μm liquid drops on the metallic surfaces of as-prepared (a–c) Ti/Cu/Ti/Si thin film wetted with deionized water, diiodomethane, and ethylene glycol, respectively, and (d–f) Ti/Zr/Ti/Si thin film wetted in the same order. Ti is the uppermost layer.

Thin Ti-based films (Ti/Cu/Ti and Ti/Zr/Ti), prepared using ion sputter deposition techniques and subsequently modified with a femtosecond laser pulse, were subjected to cytotoxicity testing (MTT) to gain the most realistic insight into the behavior of the tested materials in the human body. The viability of MRC-5 cells in contact with the tested materials after 24 h is shown in Figure 6a. The lowest mean value of viability of about 85% was observed on the laser-irradiated surface of Ti/Cu/Ti/Si in a medium diluted to 50%. Meanwhile, MRC-5 cells on the surface of Ti/Zr/Ti/Si showed a higher mean viability value of over 100% compared to a control sample. The following order represents the ranking of the materials based on the percentage of MRC-5 cells surviving over the

selected time period: 100% Ti/Zr/Ti > 15% Ti/Zr/Ti > 50% Ti/Zr/Ti > 100% Ti/Cu/Ti > 15% Ti/Cu/Ti > 50% Ti/Cu/Ti. However, after 24 h, the degree of survival of cells in contact with pure Ti materials is roughly similar to, or greater than, the degree of survival of cells in contact with the control material. The typical value of viability after 24 h is between 102 and 107%.

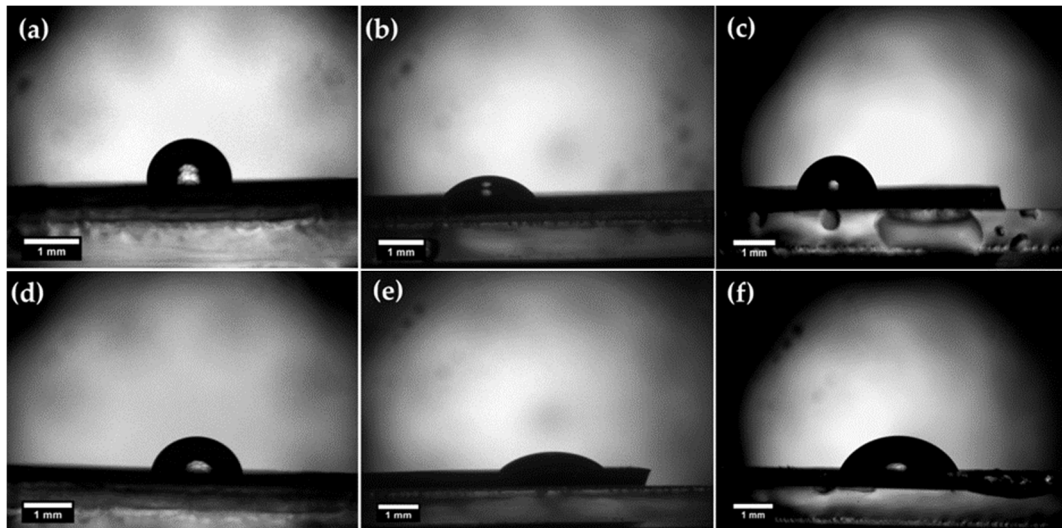


Figure 5. Static behavior of 3 μm liquid drops on the metallic surfaces after femtosecond laser irradiation for (a–c) Ti/Cu/Ti/Si thin film wetted with deionized water, diiodomethane, and ethylene glycol, respectively, and (d–f) Ti/Zr/Ti/Si thin film wetted in the same order.

It can be concluded that the mean viability of MRC-5 cells in indirect contact with all tested materials exceeds the mean viability of cells in contact with the control material. On the surface of all materials tested, MRC-5 cells had a typical triangular, elongated spindle, and star form with conspicuous cytoplasmic appendages (Figure 6b). The results demonstrated that both tested groups of materials have appropriate biocompatibility and are safe for use in the human body. The results of the conducted MTT test showed that the materials obtained by the method of cathodic sputtering and modified by laser rays are not cytotoxic.

It is common for the laser modification of metallic materials to lead to the formation of nanoparticles as a result of the condensation of the ablated material. In particular, the higher number of formed nanoparticles with a wide range of dimensions appears during the irradiation by femtosecond laser pulses due to the weak pronounced hydrodynamic effects on the sample surface [28,32,33]. Metallic nanoparticles show a wide range of positive effects on stem cell differentiation and have a number of applications in regenerative medicine. However, metallic nanoparticles also have negative effects on stem cells in several ways. One of the common mechanisms is through the production of reactive oxygen species (ROS), which can cause oxidative stress and damage to cellular components such as proteins, lipids, and DNA. Nanoparticles can also disrupt cellular membranes and alter cellular signaling pathways, leading to changes in cell behavior and function. In addition, nanoparticles can accumulate in cells and tissues, potentially leading to toxicity over time. The specific mechanisms by which nanoparticles affect cells can vary depending on the properties of the nanoparticles themselves, as well as the type of cell and tissue they are interacting with [53,54]. The negative effects of nanoparticle–cell interactions depend on several factors such as the size, shape, surface charge, and surface chemistry of the nanoparticles. The interaction between the nanoparticles and the cell membrane can lead to the internalization of the nanoparticles by the cell. The process can occur through several pathways such as endocytosis, phagocytosis, or direct penetration of the cell membrane [55]. Nanoparticles of TiO_2 showed a toxic effect in MSCs in a size-

dependent manner, which was highlighted by low cell migration, a lack of cell membrane integrity, and the suppression of osteogenic differentiation [56]. In addition, nanotubes of TiO₂ larger than 50 nm showed a drastic decrease in the proliferation and differentiation of MSCs [56]. Nanoparticles on the titanium implant can affect the biological function of the surrounding cells in two ways, firstly by affecting protein adsorption around cells and secondly by penetrating cells directly. The degree of this effect in both cases depends on particle size and nanopography. The results confirmed that the TiO₂ nanoparticles (15–200 nm) had a cytotoxic effect on MSCs depending on their concentration. This finding could be interpreted to show that highly concentrated TiO₂ nanoparticles produce oxidative stress as well as reactive oxygen species, leading to cell death. Furthermore, it was observed that the growth and division of MSCs were negatively affected in a size-dependent manner by the TiO₂ nanoparticles potentially via a mechanism causing intracellular acidity, thus inhibiting cell proliferation [56]. In our experiment, no decrease in the number of cells was observed, probably due to the additional preparation of samples before cell cultivation, or the number and dimension of laser-produced nanoparticles being below a critical value, which would negatively affect the number of surviving cells.

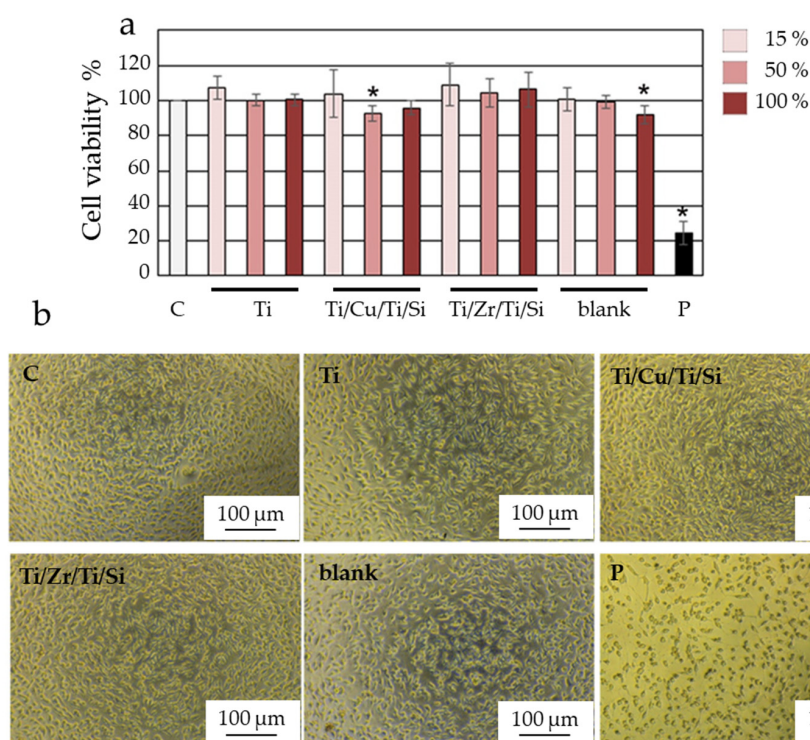


Figure 6. Cytotoxic assay of Titanium films on MRC5 cells. **(a)** Histogram representation of the effect of titanium films on MRC-5 viability, quantified following four independent experiments with technical replicates. The relative cytotoxic effect of titanium films was calculated as a percentage of surviving cells upon treatment with three different concentrations of an extraction medium obtained from the incubated titanium films with DMEM for 10 days at 37 °C compared to cells treated with fresh DMEM (designed as C) that was set as 100%. MRC-5 cells treated with DMEM incubated for 10 days at 37 °C without films (designed as Blank) were used as an additional control. As a positive control for cytotoxicity, we used MRC-5 cells treated with pyrimethanil (designed as P). Results are presented as the means \pm SEM of four independent experiments. *p* values were calculated using Student's *t*-test, * *p* \leq 0.05. **(b)** MRC5 cells 24 h after treatment with an extraction medium obtained from the incubated titanium films with DMEM for 10 days at 37 °C. Cells treated with fresh DMEM (designed as C) were used as control. As a positive control for cytotoxicity MRC-5 cells were used, treated with pyrimethanil (designed as P). Cells were monitored under a microscope at a magnification of 20 \times .

It was confirmed that laser-processed Zr-based materials are capable of modulating cell attachment, alignment, and proliferation and that hMSCs undergo a faster and greater osteogenic differentiation, even when cultured with non-supplemented media [13]. Jiao et al. found that MG63 osteoblast-like cells on the groove-textured surface of the Ti–Zr alloy exhibited higher viability and better adhesion compared to those on the original untextured surfaces [57]. They suggested that the higher surface roughness, the increased presence of metallic oxides, and the enhanced hydrophilicity of the groove-textured sample were the main contributors to its improved cytocompatibility. Busuioc et al. conducted a biocompatibility evaluation on MSCs cells via the cell proliferation assay (MTT) for Ti–Zr substrates, which indicates a lack of cytotoxicity [58]. Here, cell proliferation is favored and cells can survive in the long term. The fluorescence microscopy images show the normal development of the cells, which maintain their shape and have an unchanged metabolism. In accordance with these and our current results regarding the laser-processed Ti/Zr multilayer thin films, from a biological point of view, these systems show an improved ability to sustain cell survival and promote cell proliferation as well as cell orientation along laser-induced periodic surface structures.

4. Conclusions

The bioactive surface of Ti-based thin films, which improves cell viability, was achieved by depositing Ti/Zr/Ti/Si and Ti/Cu/Ti/Si systems and using ultrafast laser processing. The micro- and nanometer morphological features in the form of arranged patterns were obtained by laser-printed lines incorporated into a regular mesh of a 5 mm × 5 mm area. A laser-induced periodic surface structure (LIPSS) is formed in the laser-printed lines, which is oriented normal to the polarization of the laser beam and defined as low spatial frequency LIPSS (LSFL). The different width of the lines (wider for the Ti/Zr/Ti/Si system) is a consequence of the different degree of material removal during laser irradiation. An analysis of the elemental composition at specific points on the modified surface, as well as the mapping of the surface to determine the distribution of components, led to the conclusion that more intense material removal was obtained for the Ti/Zr/Ti/Si system, whereas for the Ti/Cu/Ti/Si, the surface oxidation was somewhat more pronounced.

The biocompatibility of the laser-textured Ti/Zr/Ti/Si and Ti/Cu/Ti/Si systems was determined based on the viability of MRC-5 cells in indirect contact with the samples. The results clearly show that both tested thin-film systems have adequate biocompatibility and are safe for use in the human body. The results of the MTT test show that these materials are not cytotoxic, and the typical value of viability after 24 h is more than 100%. The bioactivation of these specific multilayer systems with laser surface texturing and the tailoring of surface morphology and wettability could be useful for tissue engineering and implant applications.

Author Contributions: Conceptualization, S.P., M.J.S. and E.S.; methodology, N.B., V.R., D.K. and D.S.N.; validation, S.P., M.J.S. and E.S.; formal analysis, N.B., V.R., D.S.N. and D.K.; investigation, S.P. and N.B.; writing—original draft preparation, S.P., D.S.N. and N.B.; writing—review and editing, S.P.; supervision, S.P. All authors have read and agreed to the published version of the manuscript.

Funding: This research was funded by the EU-H2020 Research and Innovation Program under the grant agreement NFFA-Europe-Pilot (n. 101007417), having benefitted from the access provided by the Foundation for Research and Technology Hellas (FORTH) access provider (Institute of Electronic Structure and Lasers, i.e., Institution) in Heraklion, Crete, Greece, within the framework of the NFFA-Europe Transnational Access Activity.

Institutional Review Board Statement: Not applicable.

Informed Consent Statement: Not applicable.

Data Availability Statement: Not applicable.

Acknowledgments: This work was supported by the Ministry of Science, Technological Development and Innovation of the Republic of Serbia (projects No. 451-03-47/2023-01/200017 and No. 451-03-

47/2023-01/200042). We also acknowledge the support from the European Community, COST Action project no. CA21159 (PhoBios).

Conflicts of Interest: The authors declare no conflict of interest.

References

1. Asri, R.I.M.; Harun, W.S.W.; Samykano, M.; Lah, N.A.C.; Ghani, S.A.C.; Tarlochan, F.; Raza, M.R. Corrosion and surface modification on biocompatible metals: A review. *Mater. Sci. Eng. C* **2017**, *77*, 1261–1274. [[CrossRef](#)] [[PubMed](#)]
2. Rack, H.J.; Qazi, J.I. Titanium alloys for biomedical applications. *Mater. Sci. Eng. C* **2006**, *26*, 1269–1277. [[CrossRef](#)]
3. Shalabi, M.; Gortemaker, A.; Hof, M.V.; Jansen, J.; Creugers, N. Implant Surface Roughness and Bone Healing: A Systematic Review. *J. Dent. Res.* **2006**, *85*, 496–500. [[CrossRef](#)]
4. Szczęsny, G.; Kopec, M.; Politis, D.J.; Kowalewski, Z.L.; Łazarski, A.; Szolc, T. A Review on Biomaterials for Orthopaedic Surgery and Traumatology: From Past to Present. *Materials* **2022**, *15*, 3622. [[CrossRef](#)]
5. Benea, L.; Simionescu-Bogatu, N. Reactivity and Corrosion Behaviors of Ti6Al4V Alloy Implant Biomaterial under Metabolic Perturbation Conditions in Physiological Solutions. *Materials* **2021**, *14*, 7404. [[CrossRef](#)] [[PubMed](#)]
6. Liu, C.; Matsunami, C.; Shirosaki, Y.; Miyazaki, T. Bioactive Co-Cr alloy for biomedical applications prepared by surface modification using self-assembled monolayers and poly- γ -glutamic acid. *Dent. Mater. J.* **2015**, *34*, 707–712. [[CrossRef](#)] [[PubMed](#)]
7. Wang, L.; Xie, L.; Shen, P.; Fan, Q.; Wang, W.; Wang, K.; Lu, W.; Hua, L.; Zhang, L.-C. Surface microstructure and mechanical properties of Ti-6Al-4V/Ag nanocomposite prepared by FSP. *Mater. Charact.* **2019**, *153*, 175–183. [[CrossRef](#)]
8. Feng, J.; Wei, D.; Zhang, P.; Yu, Z.; Liu, C.; Lu, W.; Wang, K.; Yan, H.; Zhang, L.; Wang, L. Preparation of TiNbTaZrMo high-entropy alloy with tunable Young's modulus by selective laser melting. *J. Manuf. Process.* **2023**, *85*, 160–165. [[CrossRef](#)]
9. Dong, J.; Pacella, M.; Liu, Y.; Zhao, L. Surface engineering and the application of laser-based processes to stents—A review of the latest development. *Bioact. Mater.* **2022**, *10*, 159–184. [[CrossRef](#)]
10. Wang, W.; Zhang, X.; Sun, J. Phase stability and tensile behavior of metastable β Ti-V-Fe and Ti-V-Fe-Al alloys. *Mater. Charact.* **2018**, *142*, 398–405. [[CrossRef](#)]
11. Jung, I.; Jang, H.; Oh, M.; Lee, J.; Wee, D. Microstructure control of TiAl alloys containing β stabilizers by directional solidification. *Mater. Sci. Eng. A* **2002**, *A329–A331*, 13–18. [[CrossRef](#)]
12. Donato, T.A.G.; de Almeida, L.H.; Nogueira, R.A.; Niemeyer, T.C.; Grandini, C.R.; Caram, R.; Schneider, S.G.; Santos, A.R., Jr. Cytotoxicity study of some Ti alloys used as biomaterial. *Mater. Sci. Eng. C* **2009**, *29*, 1365–1369. [[CrossRef](#)]
13. Carvalho, A.; Canguero, L.; Oliveira, V.; Vilar, R.; Fernandes, M.H.; Monteiro, F.J. Femtosecond laser microstructured Alumina toughened Zirconia: A new strategy to improve osteogenic differentiation of hMSCs. *Appl. Surf. Sci.* **2018**, *435*, 1237–1245. [[CrossRef](#)]
14. Putra, N.E.; Mirzaali, M.J.; Apachitei, I.; Zhou, J.; Zadpoor, A.A. Multi-material additive manufacturing technologies for Ti-, Mg-, and Fe-based biomaterials for bone substitution. *Acta Biomater.* **2020**, *109*, 1–20. [[CrossRef](#)] [[PubMed](#)]
15. Correa, D.; Kuroda, P.; Lourenço, M.; Fernandes, C.; Buzalaf, M.; Zambuzzi, W.; Grandini, C. Development of Ti-15Zr-Mo alloys for applying as implantable biomedical devices. *J. Alloys Compd.* **2018**, *749*, 163–171. [[CrossRef](#)]
16. Zhao, D.; Chen, C.; Yao, K.; Shi, X.; Wang, Z.; Hahn, H.; Gleiter, H.; Chen, N. Designing biocompatible Ti-based amorphous thin films with no toxic element. *J. Alloys Compd.* **2017**, *707*, 142–147. [[CrossRef](#)]
17. Gordin, D.M.; Gloriant, T.; Texier, G.; Thibon, I.; Ansel, D.; Duval, J.L.; Nagel, M.D. Development of a β -type Ti-12Mo-5Ta alloy for biomedical applications: Cytocompatibility and metallurgical aspects. *J. Mater. Sci. Mater. Med.* **2004**, *15*, 885–891. [[CrossRef](#)]
18. Wang, L.; Lu, W.; Qin, J.; Zhang, F.; Zhang, D. The characterization of shape memory effect for low elastic modulus biomedical β -type titanium alloy. *Mater. Charact.* **2010**, *61*, 535–541. [[CrossRef](#)]
19. Ikarashi, Y.; Toyoda, K.; Kobayashi, E.; Doi, H.; Yoneyama, T.; Hamanaka, H.; Tsuchiya, T. Improved Biocompatibility of Titanium–Zirconium (Ti–Zr) Alloy: Tissue Reaction and Sensitization to Ti–Zr Alloy Compared with Pure Ti and Zr in Rat Implantation Study. *Mater. Trans.* **2005**, *46*, 2260–2267. [[CrossRef](#)]
20. Barter, S.; Stone, P.; Brägger, U. A pilot study to evaluate the success and survival rate of titanium-zirconium implants in partially edentulous patients: Results after 24 months of follow-up. *Clin. Oral Implant. Res.* **2011**, *23*, 873–881. [[CrossRef](#)]
21. Grandin, H.M.; Berner, S.; Dard, M. A Review of Titanium Zirconium (TiZr) Alloys for Use in Endosseous Dental Implants. *Materials* **2012**, *5*, 1348–1360. [[CrossRef](#)]
22. Liu, Z.; Liu, X.; Ramakrishna, S. Surface engineering of biomaterials in orthopedic and dental implants: Strategies to improve osteointegration, bacteriostatic and bactericidal activities. *Biotechnol. J.* **2021**, *16*, 2000116. [[CrossRef](#)] [[PubMed](#)]
23. Wu, W.; Cheng, R.; das Neves, J.; Tang, J.; Xiao, J.; Ni, Q.; Liu, X.; Pan, G.; Li, D.; Cui, W.; et al. Advances in biomaterials for preventing tissue adhesion. *J. Control. Release* **2017**, *261*, 318–336. [[CrossRef](#)] [[PubMed](#)]
24. Frostevarg, J.; Olsson, R.; Powell, J.; Palmquist, A.; Brånemark, R. Formation mechanisms of surfaces for osseointegration on titanium using pulsed laser spattering. *Appl. Surf. Sci.* **2019**, *485*, 158–169. [[CrossRef](#)]
25. Berg, Y.; Kotler, Z.; Shacham-Diamand, Y. Holes generation in glass using large spot femtosecond laser pulses. *J. Micromech. Microeng.* **2018**, *28*, 035009. [[CrossRef](#)]
26. Jenko, M.; Gorenšek, M.; Godec, M.; Hodnik, M.; Batič, B.; Donik, Č.; Grant, J.T.; Dolinar, D. Surface chemistry and microstructure of metallic biomaterials for hip and knee endoprostheses. *Appl. Surf. Sci.* **2018**, *427*, 584–593. [[CrossRef](#)]

27. Simitzi, C.; Ranella, A.; Stratakis, E. Controlling the morphology and outgrowth of nerve and neuroglial cells: The effect of surface topography. *Acta Biomater.* **2017**, *51*, 21–52. [CrossRef]
28. Bonse, J.; Koter, R.; Hartelt, M.; Spaltmann, D.; Pentzien, S.; Höhm, S.; Rosenfeld, A.; Krüger, J. Tribological performance of femtosecond laser-induced periodic surface structures on titanium and a high toughness bearing steel. *Appl. Surf. Sci.* **2015**, *336*, 21–27. [CrossRef]
29. Gniliyskiy, I.; Derrien, T.J.-Y.; Levy, Y.; Bulgakova, N.M.; Mocek, T.; Orazi, L. High-speed manufacturing of highly regular femtosecond laser-induced periodic surface structures: Physical origin of regularity. *Sci. Rep.* **2017**, *7*, 8485. [CrossRef]
30. Kirner, S.V.; Wirth, T.; Sturm, H.; Krüger, J.; Bonse, J. Nanometer-resolved chemical analyses of femtosecond laser-induced periodic surface structures on titanium. *J. Appl. Phys.* **2017**, *122*, 104901. [CrossRef]
31. Li, C.L.; Fisher, C.J.; Burke, R.; Andersson-Engels, S. Orthopedics-Related Applications of Ultrafast Laser and Its Recent Advances. *Appl. Sci.* **2022**, *12*, 3957. [CrossRef]
32. Stasić, J.; Gaković, B.; Perrie, W.; Watkins, K.; Petrović, S.; Trtica, M. Surface texturing of the carbon steel AISI 1045 using femtosecond laser in single pulse and scanning regime. *Appl. Surf. Sci.* **2011**, *258*, 290–296. [CrossRef]
33. Petrović, S.; Peruško, D.; Kovač, J.; Panjan, P.; Mitrić, M.; Pjević, D.; Kovačević, A.; Jelenković, B. Design of co-existence parallel periodic surface structure induced by picosecond laser pulses on the Al/Ti multilayers. *J. Appl. Phys.* **2017**, *122*, 115302. [CrossRef]
34. Babaliari, E.; Kavatzikidou, P.; Angelaki, D.; Chaniotaki, L.; Manousaki, A.; Siakouli-Galanopoulou, A.; Ranella, A.; Stratakis, E. Engineering Cell Adhesion and Orientation via Ultrafast Laser Fabricated Microstructured Substrates. *Int. J. Mol. Sci.* **2018**, *19*, 2053. [CrossRef]
35. Kovačević, A.G.; Petrović, S.; Petrović, S.; Mimidis, A.; Stratakis, E.; Pantelić, D.; Kolaric, B. Molding wetting by laser-induced nanostructures. *Appl. Sci.* **2020**, *10*, 6008. [CrossRef]
36. Petrović, S.; Peruško, D.; Mimidis, A.; Kavatzikidou, P.; Kovač, J.; Ranella, A.; Novaković, M.; Popović, M.; Stratakis, E. Response of NIH 3T3 fibroblast cells on laser-induced periodic surface structures on a 15×(Ti/Zr)/Si multilayer system. *Nanomaterials* **2020**, *10*, 2531. [CrossRef]
37. Amigó-Mata, A.; Haro-Rodriguez, M.; Vicente-Escuder, Á.; Amigó-Borrás, V. Development of Ti–Zr alloys by powder metallurgy for biomedical applications. *Powder Met.* **2021**, *65*, 31–38. [CrossRef]
38. Liu, J.; Zhang, X.; Wang, H.; Li, F.; Li, M.; Yang, K.; Zhang, E. The antibacterial properties and biocompatibility of a Ti–Cu sintered alloy for biomedical application. *Biomed. Mater.* **2014**, *9*, 025013. [CrossRef]
39. Zhang, E.; Wang, X.; Chen, M.; Hou, B. Effect of the existing form of Cu element on the mechanical properties, bio-corrosion and antibacterial properties of Ti–Cu alloys for biomedical application. *Mater. Sci. Eng. C* **2016**, *69*, 1210–1221. [CrossRef]
40. National Institute of Health, USA. Available online: <https://rsb.info.nih.gov/ij/> (accessed on 28 March 2023).
41. Van Oss, C.J.; Chaudhury, M.K.; Good, R.J. Monopolar surfaces. *Adv. Colloid Interface Sci.* **1987**, *28*, 35–64. [CrossRef]
42. Aleksić, M.; Stanisavljević, D.; Smiljković, M.; Vasiljević, P.; Stevanović, M.; Soković, M.; Stojković, D. Pyrimethanil: Between efficient fungicide against *Aspergillus* rot on cherry tomato and cytotoxic agent on human cell lines. *Ann. Appl. Biol.* **2019**, *175*, 228–235. [CrossRef]
43. Gastaldi, D.; Baleani, M.; Fognani, R.; Airaghi, F.; Bonanni, L.; Vena, P. An experimental procedure to perform mechanical characterization of small-sized bone specimens from thin femoral cortical wall. *J. Mech. Behav. Biomed. Mater.* **2020**, *112*, 104046. [CrossRef] [PubMed]
44. Lee, S.H.; Kwon, S.Y.; Ham, H.J. Thermal conductivity of tungsten–copper composites. *Thermochim. Acta* **2012**, *542*, 2–5. [CrossRef]
45. Klemens, P.G.; Williams, R.K. Thermal conductivity of metals and alloys. *Int. Met. Rev.* **1986**, *31*, 197–215. [CrossRef]
46. Petrović, S.; Peruško, D.; Skoulas, E.; Kovač, J.; Mitrić, M.; Potočnik, J.; Rakočević, Z.; Stratakis, E. Laser-Assisted Surface Texturing of Ti/Zr Multilayers for Mesenchymal Stem Cell Response. *Coatings* **2019**, *9*, 854. [CrossRef]
47. Petrović, S.; Tsihidis, G.D.; Kovačević, A.; Božinović, N.; Peruško, D.; Mimidis, A.; Manousaki, A.; Stratakis, E. Effects of static and dynamic femtosecond laser modifications of Ti/Zr multilayer thin films. *Eur. Phys. J. D* **2021**, *75*, 304. [CrossRef]
48. Kisić, D.; Nenadović, M.; Barudžija, T.; Noga, P.; Vaňa, D.; Muška, M.; Rakočević, Z. Modification of polyethylene’s surface properties by high fluence Fe implantation. *Nucl. Instrum. Methods Phys. Res. Sect. B Beam Interact. Mater. Atoms* **2020**, *462*, 143–153. [CrossRef]
49. Vogler, E.A. Structure and reactivity of water at biomaterial surfaces. *Adv. Colloid Interface Sci.* **1998**, *74*, 69–117. [CrossRef]
50. Xu, L.-C.; Siedlecki, C.A. Effects of surface wettability and contact time on protein adhesion to biomaterial surfaces. *Biomaterials* **2007**, *28*, 3273–3283. [CrossRef]
51. Monfared, A.; Faghihi, S.; Karami, H. Biocorrosion and surface wettability of Ni-free Zr-based bulk metallic glasses. *Int. J. Electrochem. Sci.* **2013**, *8*, 7744–7752.
52. Xiao, K.; Wen, L.; Jiang, L. *Bioinspired Super Wettability Materials*; Wiley Online Library: Hoboken, NJ, USA, 2016.
53. Zhigarkov, V.; Volchkov, I.; Yusupov, V.; Chichkov, B. Metal Nanoparticles in Laser Bioprinting. *Nanomaterials* **2021**, *11*, 2584. [CrossRef]
54. Abdal Dayem, A.; Lee, S.B.; Cho, S.-G. The Impact of Metallic Nanoparticles on Stem Cell Proliferation and Differentiation. *Nanomaterials* **2018**, *8*, 761. [CrossRef]
55. Medici, S.; Peana, M.; Pelucelli, A.; Zoroddu, M.A. An updated overview on metal nanoparticles toxicity. *Semin. Cancer Biol.* **2021**, *76*, 17–26. [CrossRef] [PubMed]

56. Cai, K.; Hou, Y.; Li, J.; Chen, X.; Hu, Y.; Luo, Z.; Ding, X.; Xu, D.; Lai, M. Effects of titanium nanoparticles on adhesion, migration, proliferation, and differentiation of mesenchymal stem cells. *Int. J. Nanomed.* **2013**, *8*, 3619–3630. [[CrossRef](#)] [[PubMed](#)]
57. Jiao, Y.; Brousseau, E.; Ayre, W.N.; Gait-Carr, E.; Shen, X.; Wang, X.; Bigot, S.; Zhu, H.; He, W. In vitro cytocompatibility of a Zr-based metallic glass modified by laser surface texturing for potential implant applications. *Appl. Surf. Sci.* **2021**, *547*, 149194. [[CrossRef](#)]
58. Busuioc, C.; Voicu, G.; Zuzu, I.D.; Miu, D.; Sima, C.; Iordache, F.; Jinga, S.I. Vitroceramic coatings deposited by laser ablation on Ti-Zr substrates for implantable medical applications with improved biocompatibility. *Ceram. Int.* **2017**, *43*, 5498–5504. [[CrossRef](#)]

Disclaimer/Publisher’s Note: The statements, opinions and data contained in all publications are solely those of the individual author(s) and contributor(s) and not of MDPI and/or the editor(s). MDPI and/or the editor(s) disclaim responsibility for any injury to people or property resulting from any ideas, methods, instructions or products referred to in the content.